Relating intermodulation distortion to the generating nonlinearity for high-temperature superconductor microwave experiments

R. Hott,* A. G. Zaitsev, and R. Schneider
Forschungszentrum Karlsruhe, Institut für Festkörperphysik, P.O. Box 3640, D-76021 Karlsruhe, Germany
(Received 21 January 2005; revised manuscript received 21 September 2005; published 7 December 2005)

We demonstrate how to derive from the intermodulation distortion (IMD) measured as a function of signal power the respective relative increase function $\Delta Z/Z_0$ of the governing nonlinear response function Z. We apply this approach to our IMD investigations on the microwave properties of high-temperature superconductors (HTS) and show how the experimental input and output quantities can be related to their theoretical model counterparts. The quantitative comparison of $\Delta Z/Z_0$ with the relative increase of the hf surface resistance $\Delta R_S/R_{S0}$ and of the hf surface reactance $\Delta X_S/X_{S0}$, both measured as functions of hf power, allows us to conclude that the IMD generation in HTS must be predominantly due to the hf-power-induced increase ΔR_S, with a negligible respective contribution from ΔX_S.

DOI: 10.1103/PhysRevB.72.214507 PACS number(s): 74.25.Nf, 02.30.Lt, 74.78.Bz

I. INTRODUCTION

Microwave experiments have played a prominent role in the investigation of the superconducting state of the high-temperature superconductors (HTS), giving first convincing evidence of a non-s-wave superconducting order parameter.[1] The HTS microwave conductivity thus does not follow the classical Mattis-Bardeen s-wave BCS behavior.[2] However, the simple two-fluid model provides an amazingly good phenomenological description of the microwave transport data in terms of the normal and superconducting fractions $f_n(T)$ and $f_s(T)=1-f_n(T)$, respectively, which are more or less universal functions of temperature T for all HTS, and a sample-dependent quasiparticle relaxation time function $\tau(T)$.[3,4] Hirschfeld *et al.* demonstrated that this behavior can be microscopically understood in terms of a BCS $d_{x^2-y^2}$ superconductor model with strong impurity-induced elastic quasiparticle scattering in combination with inelastic scattering by antiferromagnetic spin fluctuations,[5] even if the details of this meanwhile widely accepted microscopic description are still under theoretical refinement (e.g., see Ref. 6, and references cited therein).

The fact that the Drude model works out so well for the quasiparticles in the HTS superconducting state, with relaxation times as derived from microwave absorption,[3] thermal conductivity,[7] and even optical pump-prove experiments[8] exhibiting a very similar magnitude and temperature dependence, is truly amazing since the so-called normal state of HTS is still far off from a satisfactory theoretical description:[9,10] The transition into the superconducting state seems to release quasiparticles which are readily describable in terms of the d-wave BCS theory, and thus apparently involves a much more complicated process than a simple condensation of already existing normal state fermions as in the case of classical superconductors. In the microwave experiments and their two-fluid evaluation, this transition scenario becomes manifest in the rapid suppression of the quasiparticle scattering below the superconduction transition temperature T_c.[11] In the highest-purity samples at low temperature, the mean-free path ℓ possibly exceeds already the London penetration depth λ so that the electrodynamic treatment of HTS as superconductors in the local limit may have to be modified by taking nonlocal effects into consideration.[3,12] Due to the extremely small coherence length $\xi \sim 1$ nm, HTS are well described in terms of the clean limit $\xi \ll \ell$. This is again in striking contrast to their normal state properties where a Drude model description comes up with subatomic mean-free path lengths.[13]

The basic quantities to be measured in microwave experiments are the surface resistance R_S, quantifying the dissipation in the superconductor, and the surface reactance X_S, describing the expulsion of magnetic fields from the superconductor. In contrast to metals with $R_S=X_S$, for superconductors the dissipative response is much weaker than the reactive one

$$R_S \ll X_S \tag{1}$$

(Ref. 14), e.g., in our HTS experiments we find $X_S \approx 100 \cdot R_S$.

Subjecting superconducting samples to strong microwave (hf) fields, e.g., in resonators and filters,[15,16] introduces a sizable increase of the surface resistance ΔR_S as well as that of the surface reactance ΔX_S. For HTS one observes that these increases are of the same order of magnitude[16–18]

$$\Delta R_S \sim \Delta X_S. \tag{2}$$

Furthermore, this nonlinear behavior as a function of applied hf power introduces mixing of hf signals at neighboring frequencies. This signal distortion effect is usually characterized in two-tone intermodulation distortion (IMD) experiments observing the hf spectrum induced by irradiation of two hf signals of equal amplitude at neighboring frequencies as a function of applied hf power.[19–22]

The physical explanation and mathematical modeling of the nonlinear behavior of this effect is still a subject of controversy. It has been attributed to the hf-power-induced increase either of the surface resistance R_S,[17] or the respective increase of the surface reactance X_S. Model calculations of the relation between these quantities and the intensity of the

lowest order peaks of the IMD spectrum ("IMD3") (Refs. 19–22) have demonstrated that both suggestions provide a plausible mechanism, but could not give a decisive argument in favor of one of these hypotheses. Besides the principal physical question, the answer to this problem has become one of metrological relevance since IMD measurements have already been used to determine the lowest nonlinear correction to the penetration depth $\Delta\lambda$ of HTS via IMD measurement assuming $\Delta X_S = \omega\mu\Delta\lambda$ as the physical origin of IMD,[23] even if by means of (2) this approach can be expected to lead to an at least approximately correct relation anyway.

We suggest a route of how to solve the IMD origin problem by means of a phenomenological IMD response function Z which relates the input and output quantities of respective experiments. Our approach allows us to calculate from IMD data the relative increase of this response function $\Delta Z/Z_0 = [Z - Z_0]/Z_0$ as a function of hf power. Assuming a reasonable functional dependence of Z on R_S and X_S, the quantitative comparison of this function with the relative increases of both R_S and X_S measured in our HTS resonator experiments[24,25] is sufficient to conclude that the hf-power-induced increase of R_S is the dominating IMD generating nonlinearity mechanism with only a negligible contribution due to X_S.

We want to point out that our approach can be applied to *any* kind of IMD response in order to reconstruct the relative increase $\Delta Z/Z_0 = [Z - Z_0]/Z_0$ of the governing response function and to clarify in this way if a physical quantity, which is suspected to give rise to the IMD, actually provides a sufficiently strong nonlinear mechanism that can quantitatively explain the observed IMD generation.

An important issue for the practical applicability of our approach is the identification of the experimental input and output quantities with the respective functions used in our response function ansatz. We developed a strategy that achieves this identification without reference to possibly misleading physical modeling.

II. TWO-TONE INTERMODULATION

Following previous approaches[19–22] we start out by relating the output hf field E with the input hf field H in terms of a response function Z by

$$E(H) = Z(H)H, \tag{3}$$

however, without any reference to an electric or magnetic nature of these fields: In contrast to the previous approaches we do not equate Z either with the real (R_S) or the imaginary (X_S) part of the surface resistance Z_S. The assumption $P_{circ}(H) \propto H^2$ provided in these previous approaches the connection of H with the hf power circulating in the resonator P_{circ} as the actual experimental input variable. The nth order IMD output power was then finally obtained from the respective Fourier component of the electric output field as

$$P_n(H) \propto |E_n(H)|^2. \tag{4}$$

This computational scheme predicts for low hf power $P_{n=0} \propto H^2 \propto P_{circ}$ for the fundamental mode, $P_{n=1} \propto H^6 \propto P_{circ}^3$ for the third-order IMD, $P_{n=2} \propto H^{10} \propto P_{circ}^5$ for the fifth-order IMD, and so forth as we will see in (8). However, in most cases the experimental data, e.g., Fig. 1, show clear deviations from this prediction.[17] Moreover, energy conservation does not allow these relations to hold true for arbitrarily high hf power since the total output power $P_{out} = \Sigma P_n$ would have to increase much stronger than P_{circ}. Renormalization of the power distribution among the IMD channels is therefore expected. Physically, this amounts to a feedback of the output on the input field which substantially modifies the $P_{circ}(H)$ dependency as we will show in the following.

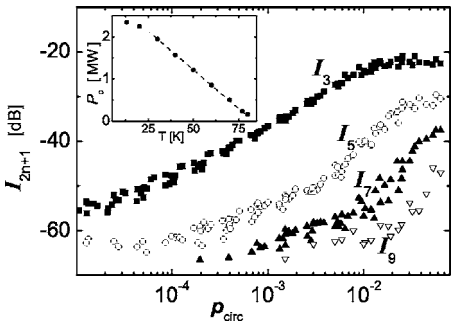

FIG. 1. IMD power ratios I_3, I_5, I_7 of a HTS disk resonator measured at various temperatures $T = 13-80$ K as a function of the normalized circulating hf power $p_{circ} = P_{circ}/P_c(T)$. Inset: Experimentally derived hf power scaling function $P_c(T)$.

Instead of selecting $Z = R_S$ or $Z = X_S$ we start in (3) with an unspecified response function

$$Z(H) = \sum_{m=0}^{\infty} Z_m H^m \tag{5}$$

and derive information about the coefficients Z_m and the $P_{circ}(H)$ dependency from experiments based on various types of hf input fields $H(t)$.

IMD measurements use a two-tone input ($\omega = \omega_0 \pm \delta_0$)

$$H(t) = H_0 \cos(\omega_0 t)\cos(\delta_0 t) \tag{6}$$

with a carrier frequency ω_0 and a modulation frequency $\delta_0 \ll \omega_0$.[26] Inserting (6) in (3) and (5) and filtering out the frequency range $\omega \approx \omega_0$ we obtain (see Appendix A)

$$E[H_0](t) = 4\cos(\omega_0 t)\sum_{n=0}^{\infty} E_n(H_0)\cos((2n+1)\delta_0 t), \tag{7}$$

$$E_n(H_0) = H_0^{2n+1}\sum_{l=0}^{\infty} z_{n+l}\binom{2(n+l)+1}{l} H_0^{2l}, \tag{8}$$

$$z_m = Z_{2m}\binom{2m+1}{m} \Big/ 4^{2m+1}. \tag{9}$$

The coefficients Z_{2n+1} do not give any contribution here. From time reversal symmetry arguments we expect

$$Z_{2n+1} = 0. \tag{10}$$

We will show in the next section that (10) can be tested experimentally and has been verified for appropriate physical

conditions. According to (8) and (9) the coefficients Z_{2n} can, in principle, be determined from the complex amplitude $E_n(H_0 \to 0)$. Our measurements give experimental access only to the IMD power ratios

$$I_{2n+1}(H_0) = P_n(H_0)/P_0(H_0). \tag{11}$$

With the definition of the critical field amplitude for the onset of the nonlinear response regime

$$\bar{H} = |3Z_2/Z_0|^{-1/2} = |16 z_1/z_0|^{-1/2} \tag{12}$$

we can express the input field amplitude and the response function coefficients in a dimensionless notation as

$$h = |z_1/z_0|^{1/2} H_0 = H_0/(4\bar{H}), \tag{13}$$

$$c_n = (z_n/z_0)/|z_1/z_0|^n = \binom{2n+1}{n} Z_{2n} \bar{H}^{2n}/Z_0. \tag{14}$$

From (4) and (8) we derive

$$I_{2n+1}(h) = h^{4n} |T_n(h)/T_0(h)|^2, \tag{15}$$

$$T_n(h) = \sum_{l=0}^{\infty} c_{n+l} \binom{2(n+l)+1}{l} h^{2l}. \tag{16}$$

With $c_0 = 1 = |c_1|$ fixed by (14), the IMD functions

$$i_{2n+1}(h) = I_{2n+1}(h)/[I_3(h)]^n, \tag{17}$$

$$= |T_n(h)|^2 [|T_0(h)|^{2(n-1)}/|T_1(h)|^{2n}], \tag{18}$$

$$= |c_n|^2 + O(h^2), \tag{19}$$

should allow us to determine $|c_{n>1}| = [i_{2n+1}(h \to 0)]^{1/2}$ in the limit of low hf power. Even without phase information on $\arg(c_{n>0})$, (15) and $c_0 = 1 = |c_1|$ provide us with

$$I_3(h) = h^4 + O(h^6), \tag{20}$$

$$h(P_{circ}) \approx [I_3(P_{circ})]^{1/4}; \tag{21}$$

a first approximation of how to relate the normalized magnetic field h to the experimental input P_{circ} by means of the measured $I_3(P_{circ})$. Further refinement of the approximation (20) will then be used to improve $h(P_{circ})$.

For technical simplification as well as for physical insight, we introduce at this point the temperature scaling

$$f(P_{circ}; T) = f[p_{circ} = P_{circ}/P_c(T)] \tag{22}$$

that we notified in our experiments on microstrip and disk resonators prepared from $YBa_2Cu_3O_{7-x}$ (YBCO) thin films on sapphire substrates[24,25] and on superconducting In microstrip resonators for our IMD data (Fig. 1), as well as for respective R_S and X_S data.[25] The scaling function $P_c(T)$ can be readily interpreted as critical hf power density with a similar temperature dependence as the critical current density [inset of Fig. 1; $P_c(T) \propto j_c(T)$]. With respect to our IMD investigations, the scaling (22) broadens our data base and defines the experimental range of the input variable p_{circ}.

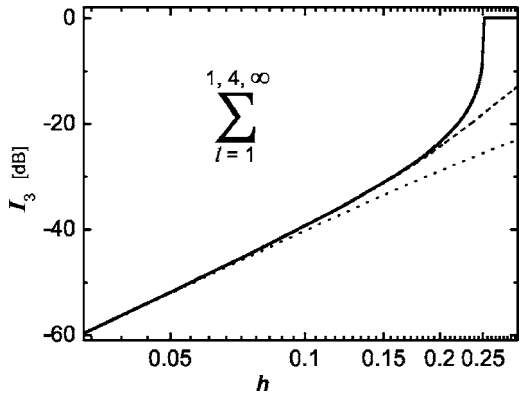

FIG. 2. $I_3(h)$ as constructed according to (15) and (16) using various approximations of (26): $I_3(h) = h^4$ ($b_{n>1} = 0$; dotted line); $b_{n=2/3/4} = 0.25/0.23/0.21$, $b_{n>4} = 0$ (dashed line); and $b_{n=2/3/4} = 0.25/0.23/0.21$, $b_{n>4} = 0.2$ (compact line).

With (22) applied to the normalized hf input field h (13) we derive $h(p_{circ})$ by comparing the measured $I_3(p_{circ})$ (Fig. 1) with the calculated $I_3(h)$ (Fig. 2). The $h(p_{circ})$ dependency that we determine with this procedure for our HTS disk resonator (Fig. 1) clearly deviates down to our lowest accessible hf power from the relation $p_{circ} \propto h^2 \Leftrightarrow P_{circ}(H) \propto H^2$, which was used as a basic equation in previous IMD derivations:[19–22] The empirical relation $I_3(p_{circ}) \propto [p_{circ}]^{1.3}$ that we find for our HTS disk resonator data in the range $10^{-5} < p_{circ} < 10^{-2}$ (Fig. 1) translates with $I_3(h) \approx h^4$ into $p_{circ} \propto h^3$. We point out that this result is not affected by the uncertainty concerning the coefficients $c_{n>0}$, since worst case estimates of possible deviations from approximation (20) based on our experimentally determined $|c_{n>0}|$ show that $I_3(h) \approx h^4$ is still an excellent approximation at least in the IMD3 range $I_3 < -40$ dB (Fig. 2). The same analysis of our HTS microstrip resonator IMD data give with $I_3(p_{circ}) \propto [p_{circ}]^{1.7} \Rightarrow p_{circ} \propto h^{2.3}$, a result which is much closer to the theoretical expectation $p_{circ} \propto h^2$. In contrast, we derived for a superconducting indium microstrip resonator of similar geometry an even larger deviation $I_3(p_{circ}) \propto [p_{circ}]^{0.9} \Rightarrow p_{circ} \propto h^{4.4}$. The functional relationship $h(p_{circ})$ thus depends both on the resonator geometry and on the superconducting material.

For a physical interpretation of these unexpected dependencies we have to give up our previous abstinence from identifying the physical nature of the input field amplitude H_0. Usually, H_0 is identified with the maximum magnetic hf field amplitude H_{max} in the resonator structure[17,27,28] which is used as a scaling parameter for the electromagnetic field distribution:

$$P_{circ} \propto \int [H(r)]^2 d^3 r = [H_{max}]^2 \int [H(r)/H_{max}]^2 d^3 r. \tag{23}$$

If the normalized integral can be assumed to not depend on H_{max} due to the linearity of the Maxwell equations this leads to the expected scaling $P_{circ} \propto [H_{max}]^2$.

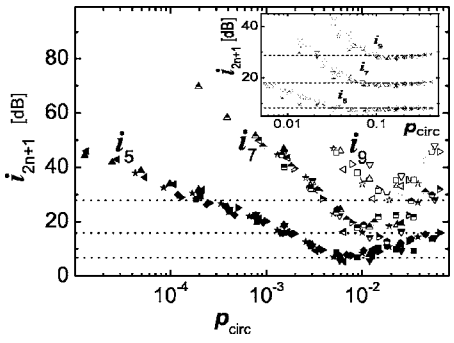

FIG. 3. IMD functions i_5, i_7, i_9 derived from the experimental HTS disk resonator data of Fig. 1. The dotted lines indicate our estimates used for the evaluation of $|c_2|$, $|c_3|$, and $|c_4|$. Inset: Respective data of a HTS microstrip resonator.

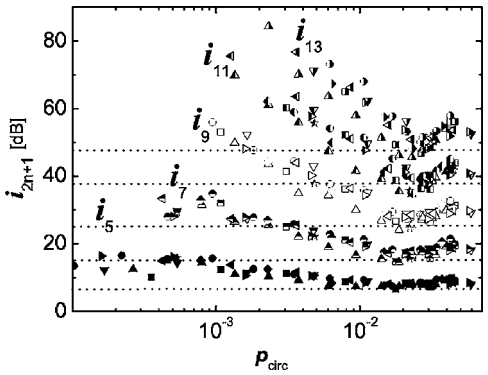

FIG. 4. IMD functions $i_{5/7/9/11/13}$ derived from experimental In microstrip resonator data. The dotted lines indicate our estimates used for the evaluation of $|c_{2/3/4/5/6}|$.

Our finding $P_{circ} \propto [H_0]^{2.3-4.4}$ indicates that our effective input field parameter H_0 as derived from the IMD activity increases at a slower rate with increasing hf power than H_{max}. Since H_{max} is not expected to be strongly influenced by the involved nonlinear mechanisms we have to consider that the IMD input field amplitude H_0 actually represents a sampling of the input field weighted according to the local IMD generation activity

$$P_{circ} \propto \int w_{IMD}(r;H_0)[H(r)]^2 d^3r. \tag{24}$$

Our result $P_{circ} \propto [H_0]^{2+\alpha}$ means that the local IMD weight factor $w_{IMD}(r;H_0)$ introduces an additional scaling $\propto [H_0]^{\alpha}$. Our idea for the reason behind this behavior is that IMD generation does neither occur in the fully superconducting nor in the fully normal conducting state: Due to the lack of an electromagnetic nonlinearity the IMD signal must arise predominantly from regions where superconductivity is driven close to its local critical limit, just before switching into a quasinormal conducting state. We approximate this situation by a model weight function which projects the regions that are exposed to a certain critical field amplitude $H_0 \pm \Delta H$. Defining the effective volume $V_{eff}(H_0)$ of these IMD-active regions such that

$$\int w_{IMD}(r;H_0)[H(r)]^2 d^3r = [H_0]^2 \times V_{eff}(H_0) \tag{25}$$

we obtain the targeted result with the physically plausible assumption that the effective IMD-active volume increases as $V_{eff}(H_0) \propto [H_0]^{\alpha}$.

We resolved for our HTS hf resonators IMDs up to the ninth order (Fig. 1) above our experimental noise floor. Applying the rules elaborated above we derived normalized IMD functions $i_{2n+1}(p_{circ})$ (19) which show a steep increase towards lower p_{circ} (Fig. 3) where we expected more or less constant values. We relate this to an IMD background that dominates small IMD signals, e.g., <-55 dB for the case of our disk resonator. This background threshold can already be distinguished in the original IMD curves from distinct kinks at this intensity level (Fig. 1). We attribute this effect to the phase noise of our measurement setup. A similar background is present in the In microstrip resonator IMD data (Fig. 4), but it is much less than in the HTS resonator data. This can be related to the substantially higher IMD signal level of In as compared to HTS. For HTS, an additional background contribution may arise from material defects where superconductivity is locally weakened ("weak links") (Ref. 29) and magnetic flux penetrates much easier than into the fully superconducting bulk with the concomitant effect of an enhanced IMD generation.

For the HTS microstrip resonator, we encounter for the IMD data in the p_{circ} range above the discussed background threshold indeed fairly constant $i_{2n+1}(p_{circ})$ (inset of Fig. 3) which justifies to identify these levels with $|c_n|^2$.[30] For the disk resonator, the $i_{2n+1}(p_{circ})$ show only a shallow minimum and an increase towards higher p_{circ}. We attribute this increase to overheating to which the extended HTS film regions of a disk resonator are much more susceptible than the narrow HTS stripes of a microstrip resonator. Nevertheless, the $|c_n|^2$ extracted as the $i_{2n+1}(p_{circ})$ minima for the disk resonator coincide with the $|c_n|^2$ extracted as the constant levels for the microstrip resonator (dotted lines in Fig. 3) and can be represented in identical parameters

$$b_n = c_n \Big/ \binom{2n+1}{n} = [Z_{2n}/Z_0]\bar{H}^{2n}, \tag{26}$$

$$|b_{2/3/4}| = 0.25/0.23/0.21 \tag{27}$$

for both HTS resonators [$b_0=1$ and $|b_1|=1/3$ by definitions (14) and (26)]. This numerical coincidence justifies our data evaluation, in agreement with our expectation that $Z(H)$ designates a materials property and does not depend on the resonator geometry which is extremely different for the two investigated resonator types. A respective analysis of the In microstrip resonator data (Fig. 4) yields with $|b_{2/3/4/5/6}| = 0.22/0.20/0.18/0.15/0.13$, significantly different parameters.

III. OTHER HF INPUT EXCITATIONS

In order to test the actual magnetic character of the hf input field H we applied our phenomenological modeling (3)

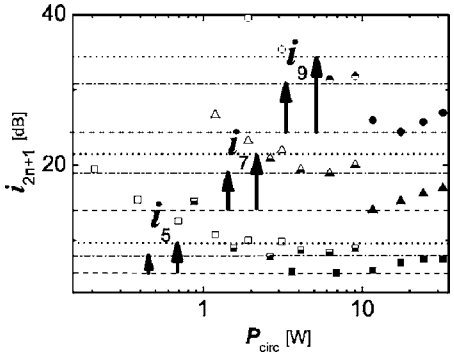

FIG. 5. Increase of the IMD functions $i_{5/7/9}$ derived for a HTS microstrip resonator under the application of a dc magnetic field of 0, 0.1, and 0.3 T plotted as a function of the (unnormalized) circulating hf power P_{circ}. The dashed, dash-dotted, and dotted lines indicate our estimates used for the evaluation of $|c_{2/3/4}|$ at 0, 0.1, and 0.3 T, respectively.

and (5) to two-tone excitation IMD experiments (6) with an additional application of a small dc magnetic field

$$H(t) = H_0 \cos(\omega_0 t)\cos(\delta_0 t) + H_{dc}. \tag{28}$$

This implies in (9) the modification (see Appendix B)

$$Z_{2n} \mapsto Z_{2n} + (2n+3)(n+1)Z_{2n+2}H_{dc}^2 + O(H_{dc}^4), \tag{29}$$

where we expect an IMD increase which is described within our theoretical formalism in terms of

$$c_n \mapsto c_n(1 + [(2n+3)(n+1)[b_{n+1}/b_n] - 3b_1]\eta) \times |1 + n[3b_1 - 10[b_2/b_1]\eta]| + O(\eta^2) \tag{30}$$

under the assumption

$$\eta = [H_{dc}/\bar{H}]^2 \ll 1, \tag{31}$$

where $\bar{H}$ is the critical nonlinearity field amplitude as defined in (12). Assuming the b_n to be real and $b_{n+1} \approx b_n$ as suggested by our HTS and In data we can obtain with

$$|c_n| \mapsto |c_n|[1 + 2(n-1)^2\eta], \tag{32}$$

in fact, a consistent description of the increasing level of the various IMD orders observed in our respective experiments with a HTS microstrip resonator (Fig. 5) using $H_{dc} \approx 0.35\bar{H}$ for an application of a dc field of 0.1 T, and $H_{dc} \approx 0.45\bar{H}$ for an application of 0.3 T, respectively. However, this nonlinear increase of the effective field parameter H_{dc} shows that there must be a considerable screening of the applied magnetic field which allows only a very rough estimate of the field parameter $\bar{H} \ll 1$ T. In order to extract quantitative information a much more detailed theory including the implications of the involved vortex dynamics[18,31] would therefore be required, which goes far beyond the level of our phenomenological description.

As a third type of hf input excitation we investigated the effect of hf irradiation at frequency ω_0 and simultaneous application of an ac magnetic field with a modulation frequency $\delta_0 \ll \omega_0$ in the range of several kHz

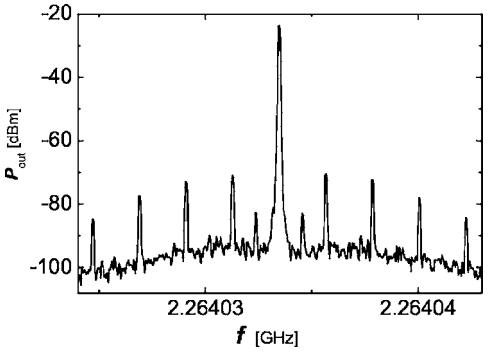

FIG. 6. Frequency spectrum emitted by an hf irradiated HTS microstrip resonator in an ac magnetic field with an amplitude $H_{ac} = 5.3$ mT.

$$H(t) = H_0 \cos(\omega_0 t) + H_{ac}\cos(\delta_0 t). \tag{33}$$

Within our model we derive for the response in the frequency range $\omega \approx \omega_0$ (see Appendix C)

$$E(t) = 2\cos(\omega_0 t)\sum_{n=-\infty}^{\infty} \bar{E}_n(H_0, H_{ac})e^{in\delta_0 t}, \tag{34}$$

where the even [odd] amplitudes are given by

$$\begin{aligned}\bar{E}_{2n[+1]}(H_0, H_{ac}) &= \sum_{l=|n|}^{\infty} [H_{ac}/2]^{2l[+1]} \binom{2l[+1]}{l-n} \\ &\quad \times \sum_{k=l}^{\infty} Z_{2k[+1]} \binom{2k[+1]+1}{2(k-l)+1} \\ &\quad \times [H_0/2]^{2(k-l)+1} \binom{2(k-l)+1}{(k-l)} \\ &= (2|n|[+1]+1)Z_{2|n|[+1]} \\ &\quad \times [H_{ac}/2]^{2|n|[+1]}[H_0/2] + \cdots . \end{aligned} \tag{35}$$

Respective experiments immediately show that the effective field parameter H_{ac} depends here in an even much more complicated manner on the amplitude of the applied external magnetic ac field $H_{ac_{applied}}$ than for the magnetic dc field: For small $H_{ac_{applied}}$, e.g., for our HTS microstrip resonator up to ~ 4.5 mT, there is no output signal at frequencies $\omega \neq \omega_0$ *at all*. Actually, the onset of the $\omega \neq \omega_0$ response is usually interpreted as an indication that the screening currents exceed the critical current density J_c and is thus used as a basic principle of a common noncontact J_c determination for superconducting films.[32]

Increasing $H_{ac_{applied}}$ above 4.5 mT we finally observe for our HTS microstrip resonator only the expected IMD-like response peaks at $\omega_0 \pm 2n\delta_0$. However, we find for 4.5 mT $< H_{ac_{applied}} < 7$ mT *additional peaks at* $\omega_0 \pm \delta_0$ (Fig. 6). Since in (35) even [odd] order response components $\bar{E}_{2n[+1]}$ are exclusively related to even [odd] order coefficients $Z_{2n[+1]}$ of the response function, the observed appearance and disappearance of additional peaks at $\omega_0 \pm \delta_0$ on the continuous increase of $H_{ac_{applied}}$ is at variance with our models (3) and

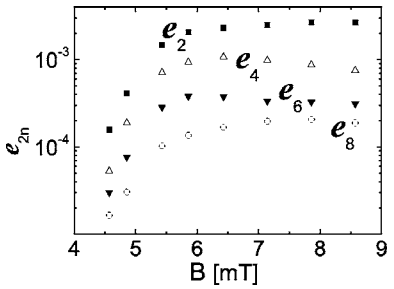

FIG. 7. Peak amplitude ratios e_{2n} derived for a HTS microstrip resonator in an ac magnetic field according to (37) plotted as functions of the ac field amplitude H_{ac}.

(5). Obviously, the hf behavior in this $H_{ac_{applied}}$ range is governed by magnetic flux penetration effects which lead to a dynamic behavior which is substantially different from the situation for higher ac fields which can easily overcome the flux penetration barrier and actually interfere with the bulk-intrinsic IMD generation mechanism.

For $H_{ac_{applied}} > 7$ mT we find in our experiments $\bar{E}_{2n+1} = 0$ and hence $Z_{2n+1} = 0$ as expected, as well as saturation behavior of the even order response components $\bar{E}_{2n}$. We take this as an indication that the applied ac field modulates at kHz frequencies the electromagnetic environment of the GHz hf waves in the superconductor. Applying our simple description in terms of (3) and (5) we rewrite (35) with (26) the amplitudes $\bar{E}_{2n}$ in this higher $H_{ac_{applied}}$ range as

$$\begin{aligned}\bar{E}_{2n}(H_0, H_{ac}) &= [H_0/2] \sum_{l=|n|}^{\infty} [H_{ac}/(2\bar{H})]^{2l} \binom{2l}{l-|n|} \\ &\times \sum_{k=l}^{\infty} b_k \binom{2k+1}{2(k-l)+1} \\ &\times [H_0/(2\bar{H})]^{2(k-l)} \binom{2(k-l)+1}{(k-l)} \\ &= (2|n|+1) b_{|n|} [H_{ac}/(2\bar{H})]^{2|n|} [H_0/2] \\ &+ O([H_{ac}/\bar{H}]^{2|n|+2}), \end{aligned} \tag{36}$$

$$\begin{aligned} e_{2n} &= |\bar{E}_{2|n|}/(2|n|+1)\bar{E}_0| \\ &= |b_{|n|}| [H_{ac}/2\bar{H}]^{2|n|} + O([H_{ac}/\bar{H}]^{2|n|+2}). \end{aligned} \tag{37}$$

The relation $e_{2n} \sim 0.001[1/2]^n$ observed for $H_{ac_{applied}} > 5$ mT (Fig. 7) in combination with the $|b_n|$ values as determined from the IMD data (27) lead to the conclusion that the value H_{ac} adjusted in this $H_{ac_{applied}}$ range cannot be described by the limit $H_{ac} \ll \bar{H}$, which would allow a practical evaluation of (37), and that H_{ac} must already be on the order of the critical field parameter $\bar{H}$ which designates the onset of a nonlinear response behavior. Since H_{ac} cannot exceed $H_{ac_{applied}}$ we conclude $2\bar{H} \sim H_{ac} \leqslant 10$ mT.

This rough estimate is in good agreement with the following consideration based on the analytical result for the circulating power of disk resonator:[33]

$$\begin{aligned} P_{circ} &= 1.77(c/[\omega_0/2\pi])(c/\mu_0)(d/\epsilon_r)(\mu_0 H_{max})^2 \\ &\approx \omega_0[\mu_0(H_{max})^2/4](\pi R^2 d), \end{aligned} \tag{38}$$

where d represents the thickness, R the radius, and ϵ_r the dielectric permitivity of the substrate. For the disk resonator shown in Fig. 1 we obtain, e.g., from $p_{circ} = 10^{-5}$ and the inset in Fig. 1 at low temperature $P_{circ} = 23$ W. With (38) for $f_0 = \omega_0/2\pi = 2.3$ GHz, $d = 0.43$ mm, $R = 2.5$ cm, and $\epsilon_r = 10$ we arrive at $H_{max} = 0.16$ mT $> H_0 = 4\bar{H}h$ as an upper limit for the effective IMD input field amplitude H_0. With $h = 0.04$ as derived from (21) or the comparison of Figs. 1 and 2 we therefore obtain $\bar{H} < 1$ mT.

Due to the unclear screening situation our hf irradiation experiments under application of a magnetic field thus allowed only a semiquantitative analysis.

IV. COMPARISON WITH R_S AND X_S

Up to now we could not clarify the actual nature of the response function Z. We will show now that the comparison of the surface resistance R_S and surface reactance X_S, the real and imaginary part of the surface impedance Z_S, respectively, with Z as a function of applied hf power actually allows us to decide about their influence on Z.

In a highly simplified theoretical picture of the experimental situation the power transferred to and dissipated in the resonator may be expressed as

$$P = [\mathrm{Re}[(E_{ant})^* H_{ant}]/2] A_{ant} \tag{39}$$

in terms of the electric (E_{ant}) and magnetic (E_{ant}) hf field at the antenna location and an effective antenna area (A_{ant}). The assumption that both hf fields are roughly proportional to their effective field amplitudes H_0 and $E_0(H_0) = Z_S(H_0)\, H_0$ at the superconductor surface leads to

$$P \propto \mathrm{Re}[Z_S(H_0)](H_0)^2 = R_S(H_0)^2. \tag{40}$$

Comparing this with the result of the signal-model approach discussed above

$$P \propto |E(H)|^2 = |Z|^2 (H_0)^2 \tag{41}$$

we come up with

$$Z \propto \sqrt{\mathrm{Re}[Z_S]} = \sqrt{R_S}. \tag{42}$$

Even if this heuristic result is only a crude approximation we may use it as a starting point for the consideration on which mathematical footing of the surface resistance R_S and surface reactance X_S must be expected to contribute to the IMD response function Z. Within our highly simplified approach X_S can only contribute to Z by means of a phase shift which could at most result in $Z \propto \sqrt{\mathrm{Re}[e^{-i\pi/2} Z_S]} = \sqrt{X_S}$. We use this heuristic dependency for a trial ansatz $Z = \varrho\sqrt{R_S} + \xi\sqrt{X_S}$ which can be linearized as

$$Z(p_{circ}) = \varrho\sqrt{R_{S0}}[2 + \Delta R_S(p_{circ}/R_{S0})] + \xi\sqrt{X_{S0}}[2 + \Delta X_S(p_{circ}/X_{S0})] \quad (43)$$

since in our experiments the observed variations of both R_S and X_S within our experimental hf power range are sufficiently small enough to justify such a linearization. The complex ϱ and ξ are subject to the restriction

$$\mathrm{Re}(\xi/\varrho) > 0 \quad (44)$$

in order to exclude unphysical compensation of dissipative and reactive response. Actually, our final result will not be restricted to the functional dependence $Z \propto \sqrt{\mathrm{Re}[Z_S]}$ but will equally apply to $Z \propto (\mathrm{Re}[Z_S])^{\alpha}$ for arbitrary α since the introduced modification of (43) will be irrelevant for our final result.

Switching with (9) and (13) back to the notation

$$4h = H/\bar{H} \quad (45)$$

$$\Delta Z(h)/Z_0 = [Z(h) - Z_0]/Z_0 = e^{1\varphi_1}\sum_{m=1}^{\infty} |b_m| e^{1(\varphi_m - \varphi_1)}[4h]^{2m} \quad (46)$$

we calculate $|\Delta Z[h(p_{circ})]/Z_0|$ under the assumption

$$\varphi_m = \varphi_1, \quad (47)$$

which sets an upper limit for $|\Delta Z[h(p_{circ})]/Z_0|$. From Figs. 1 and 2 and Eq. (27) we can estimate that the actual value of $|\Delta Z[h(p_{circ} < 10^{-3})]/Z_0|$ can be at most 10% smaller than the calculated value. From (43) we have

$$\Delta Z(p_{circ})/Z_0 = [\Delta R_S(p_{circ})/R_{S0}]/(1+\zeta) + [\Delta X_S(p_{circ})/X_{S0}]/(1+\zeta^{-1}), \quad (48)$$

$$\zeta = \xi/\varrho. \quad (49)$$

Dividing both sides of (48) by $|\Delta Z(p_{circ})/Z_0|$ results with (46) in

$$e^{1\varphi_1} = (1+\beta)/(1+\zeta) + \gamma/(1+\zeta^{-1})$$
$$\Rightarrow \zeta(1 - \gamma e^{-1\varphi_1}) = [(1+\beta)e^{-1\varphi_1} - 1]. \quad (50)$$

From

$$|\Delta Z(p_{circ})/Z_0| \approx \Delta R_S(p_{circ})/R_{S0} \sim 100[\Delta X_S(p_{circ})/X_{S0}], \quad (51)$$

in particular, for $p_{circ} < 10^{-3}$ (Fig. 8), we arrive at experimental parameters $0 < \beta, \gamma \ll 1$. It is easy to see from the graphical representation of (50) in the complex plane (Fig. 9) that $\varphi_1 \approx 0$ and $|\zeta| \ll 1$ provide the only solution which fulfills the physical requirement (44) $\mathrm{Re}(\zeta) = \mathrm{Re}(\xi/\varrho) > 0$. Hence we can draw from (48), (49), and (44) the conclusions

$$\Delta Z(p_{circ})/Z_0 \approx \Delta R_S(p_{circ})/R_{S0}, \quad (52)$$

$$\varphi_1 \approx 0. \quad (53)$$

The good agreement of (52) with the experimental data, even for $p_{circ} > 10^{-2}$ where the contributions $m = 2,3,4$ could, in principle, add up in the complex plane (46) in a way reducing the calculated upper limit of $|\Delta Z[h(p_{circ})]/Z_0|$ by more than 50% indicates that (47) represents a good approximation at least for $\varphi_{m=2,3,4}$. This permits us to refine $I_3(h)$ (20) as

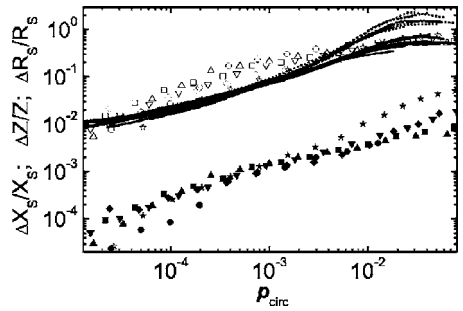

FIG. 8. HTS disk resonator surface impedance data $\Delta R_S(p_{circ})/R_{S0}$ (open symbols) and $\Delta X_S(p_{circ})/X_{S0}$ (dark symbols) compared to $|\Delta Z[h(p_{circ})]/Z_0|$ calculated without free parameter from (27) and (47) (upper dotted curves), as well as from a refined $h(p_{circ})$ approximation ($b_1 = 1/3, b_{n=2/3/4} = 0.25/0.23/0.21, b_{n>4} = 0$; lower compact curves) using the experimental $I_3(p_{circ}; T = 13 - 80\ \mathrm{K})$ curves.

$$I_3(h) = h^4 |T_1(h)/T_0(h)|^2, \quad (54)$$

$$T_n(h) = \sum_{l=0}^{\infty} b_{n+l} \binom{2(n+l)+1}{(n+l)} \binom{2(n+l)+1}{l} h^{2l}, \quad (55)$$

and thus $h(p_{circ}) = h[I_3(p_{circ})]$ based on $b_{n=0/1/2/3/4} = 1/0.33/0.25/0.23/0.21$, $b_{n>4} = 0$ (Fig. 2). The resulting $|\Delta Z(p_{circ})/Z_0|$ gives an excellent fit of $\Delta R_S(p_{circ})/R_{S0}$ without adjustable parameters (compact curves in Fig. 8). We point out that here we do not expect any substantial modification of $|\Delta Z(p_{circ})/Z_0|$ due to the undetermined coefficients $b_{n>4}$ since the difference in $|\Delta Z(h)/Z_0|$ as well as in $I_3(h)$ introduced, e.g., by the extrapolation $b_{n>4} = 0.2$ turns out to be totally negligible within our experimental data range $I_3 < -20$ dB (Fig. 2) taking the experimental scatter of our $I_3(p_{circ}, T)$ curves recorded at high p_{circ} for different T [this introduces the respective scatter of $|\Delta Z(p_{circ})/Z_0|$ in Fig. 8] into account.

If all coefficients Z_{2n} (and thus c_n and b_n) are (relatively) real one may extrapolate (27) as

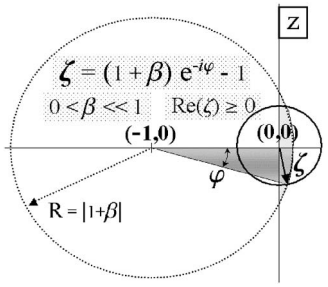

FIG. 9. Graphical representation of Eq. (50) in the complex plane [$|\gamma| \ll 1 \Rightarrow \zeta(1 - \gamma e^{-1\varphi_1}) \approx \zeta$].

$$b_n \approx ba^{2(n-1)} \tag{56}$$

to obtain a model response function

$$Z(H) \approx Z_0\left(1+\sum_{n=1}^{\infty} ba^{2(n-1)}[H/\bar{H}]^{2n}\right)$$
$$= Z_0 + Z_2H^2/(1-[aH/\bar{H}]^2), \tag{57}$$

which features a divergent behavior for $H \to \bar{H}/a \sim \bar{H}$. From (52) our estimate $\bar{H} \sim 10$ mT derived for HTS from our IMD experiments under application of an ac magnetic field is in good agreement with reported values for the critical hf amplitude for the onset of substantial R_S increase observed for high-quality HTS films.[17]

If (47) holds true for all m according to (54) and (55) $I_3(h)$ must be a monotonic increasing function. The reported observation of nonmonotonic behavior[26] implies therefore a phase change of the response function Z which could be effected by the interference of different nonlinearity mechanisms.

V. CONCLUSION

We developed a scheme for extracting information on the nonlinear response function $Z(H)$ from the output of experiments using various types of time-dependent input excitations. We extracted from two-tone intermodulation experiments on high-temperature superconductor resonators of very different geometry, apparently only materials-dependent response function parameters. We tested our response function formalism also for hf experiments with an additional application of ac or dc magnetic fields. However, the unclear screening of the external field levels here did not allow for a more than semiquantitative analysis.

From IMD, R_S and X_S measurements on a HTS hf disk resonator, we established from a direct quantitative comparison of Z, as constructed only on the basis of the intermodulation data, with the experimental surface resistance $R_S(p_{circ})$ and surface reactance $X_S(p_{circ})$ the connection $\Delta Z(p_{circ})/Z_0 \approx \Delta R_S(p_{circ})/R_{S0}$ without any indication of a substantial contribution from the surface reactance. The good agreement of our theoretical $\Delta Z(p_{circ})/Z_0$ with the measured surface resistance increase $\Delta R_S(p_{circ})/R_{S0}$ over our full hf power range shows that at least for HTS the intermodulation distortion must be caused predominantly by the hf-power-induced increase of the surface resistance ΔR_S and can stem only to a vanishing extent from the corresponding increase of surface reactance ΔX_S, even though the absolute values of these increases are roughly the same. Nevertheless, this result is in good agreement with the simple reasoning that the saturation effects of the intermodulation distortion are much more plausibly due to the substantial R_S increase $\Delta R_S \sim R_{S0}$ that we observe within our experimentally accessible hf power range rather than to the only a minute X_S increase $\Delta X_S < 0.01 X_{S0}$ that was achieved at our highest hf power level.

ACKNOWLEDGMENTS

We want to express our thanks to A. Beck, R. Smithey, and F. Ratzel for their technical support and to J. Halbritter for helpful comments and suggestions.

APPENDIX A: DERIVATION OF IMD

Singling out the $\omega = \pm\omega_0$ terms from (6) in (3) and (5) we obtain

$$E(t) = \sum_{m=0}^{\infty} Z_m[H_0(e^{\imath\omega_0 t} + e^{-\imath\omega_0 t})\cos(\delta_0 t)/2]^{m+1}$$
$$= \sum_{l=0}^{\infty}\sum_{m=0}^{\infty} Z_m[H_0\cos(\delta_0 t)/2]^{m+1}\binom{m+1}{l} e^{\imath(m+1-2l)\omega_0 t} \rightleftarrows 2\cos(\omega_0 t)\sum_{l=0}^{\infty} Z_{2l}[H_0\cos(\delta_0 t)/2]^{2l+1}\binom{2l+1}{l}$$
$$= 2\cos(\omega_0 t)\sum_{l=0}^{\infty} Z_{2l}[H_0/4]^{2l+1}\binom{2l+1}{l}\sum_{n=0}^{2l+1}\binom{2l+1}{n} e^{\imath[2n-(2l+1)]\delta_0 t}$$
$$= \cdots \sum_{n=-\infty}^{\infty}\binom{2l+1}{l-(n-l-1)} e^{\imath[2(n-l-1)+1]\delta_0 t}$$
$$= 2\cos(\omega_0 t)\sum_{n=-\infty}^{\infty}\sum_{l=0}^{\infty}\binom{2l+1}{l-n} e^{\imath(2n+1)\delta_0 t} Z_{2l}[H_0/4]^{2l+1}\binom{2l+1}{l}$$
$$= 4\cos(\omega_0 t)\sum_{n=0}^{\infty}\cos((2n+1)\delta_0 t)\sum_{l=n}^{\infty} Z_{2l}[H_0/4]^{2l+1}\binom{2l+1}{l}\binom{2l+1}{l-n}, \tag{A1}$$

where we made use of

$$\binom{n}{k} = 0 \quad \text{for } k < 0 \text{ or } k > n, \quad \binom{n}{k} = \binom{n}{n-k},$$

$$\binom{2l+1}{l-n} e^{\imath(2n+1)\delta_0 t} = \binom{2l+1}{l-(-n-1)} e^{-\imath[2(-n-1)+1]\delta_0 t}.$$

APPENDIX B: DERIVATION OF IMD IN A DC FIELD

$$\begin{aligned} E(t;H_{dc}) &= \sum_{m=0}^{\infty} Z_m [H(t)+H_{dc}]^{m+1} \\ &= \sum_{m=0}^{\infty} Z_m \{[H(t)]^{m+1} + H_{dc}(m+1)[H(t)]^m + [H_{dc}^2/2](m+1)m[H(t)]^{m-1}\} + O(H_{dc}^3) \\ &= E(t;H_{dc}=0) + \sum_{m=0}^{\infty} f_m(H_{dc})[H(t)]^m + O(H_{dc}^3), \end{aligned} \tag{B1}$$

$$f_m(H_{dc}) = (m+1)Z_m H_{dc} + (m+2)(m+1)Z_{m+1}H_{dc}^2/2 + O(H_{dc}^3). \tag{B2}$$

Singling out again the $\omega = \pm\omega_0$ terms we obtain

$$\begin{aligned} E(t;H_{dc}) - E(t;H_{dc}=0) &= \sum_{l=0}^{\infty}\sum_{m=0}^{\infty} f_m(H_{dc})[H_0\cos(\delta_0 t)/2]^m \binom{m}{l} e^{\imath(m-2l)\omega_0 t} \rightrightarrows \sum_{l=0}^{\infty} (\ldots[m=2l-1]\ldots + \ldots[m=2l+1]\ldots) \\ &= \sum_{l=1}^{\infty} f_{2l-1}(H_{dc})[H_0\cos(\delta_0 t)/2]^{2l-1}\binom{2l-1}{l} e^{-\imath\omega_0 t} + \sum_{l=0}^{\infty} f_{2l+1}(H_{dc})[H_0\cos(\delta_0 t)/2]^{2l+1}\binom{2l+1}{l} e^{\imath\omega_0 t} \\ &= 2\cos\omega_0 t \sum_{l=0}^{\infty} f_{2l+1}(H_{dc})[H_0\cos(\delta_0 t)/2]^{2l+1}\binom{2l+1}{l} \end{aligned}$$

which indicates the replacement in (A1)

$$Z_{2l} \mapsto Z_{2l} + (2l+2)Z_{2l+1}H_{dc} + (2l+3)(2l+2)Z_{2l+2}H_{dc}^2/2 + O(H_{dc}^3) = Z_{2l} + (2l+3)(2l+2)Z_{2l+2}H_{dc}^2/2 + O(H_{dc}^4), \tag{B3}$$

taking (10) into account. With $\eta = [H_{dc}/\bar{H}]^2$ and $b_0 = 1$ and $|b_1| = \frac{1}{3}$ this implies

$$\begin{aligned} b_n = c_n \Big/ \binom{2n+1}{n} = [Z_{2n}/Z_0]|3Z_2/Z_0|^{-n} &\mapsto \frac{Z_{2n} + (2n+3)(n+1)Z_{2n+2}H_{dc}^2}{Z_0 + 3Z_2H_{dc}^2} \left| \frac{Z_0 + 3Z_2H_{dc}^2}{3[Z_2 + 10Z_4H_{dc}^2]} \right|^n \\ &= \frac{b_n + (2n+3)(n+1)b_{n+1}\eta}{b_0 + 3b_1\eta} \left| \frac{(b_0 + 3b_1\eta)}{3[b_1 + 10b_2\eta]} \right|^n + O(\eta^2) \\ &= [b_n + (2n+3)(n+1)b_{n+1}\eta](1 - 3b_1\eta) \left| \frac{1}{3b_1} \right|^n \left| \frac{1 + 3b_1\eta}{1 + 10[b_2/b_1]\eta} \right|^n + O(\eta^2) \\ &= b_n(1 + \{(2n+3)(n+1)[b_{n+1}/b_n] - 3b_1\}\eta)|1 + n(3b_1 - 10[b_2/b_1]\eta)| + O(\eta^2). \end{aligned} \tag{B4}$$

APPENDIX C: DERIVATION OF IMD IN AN AC FIELD

$$H(t) = H_0\cos(\omega_0 t), \tag{C1}$$

$$B(t) = H_{ac}\cos(\delta_0 t), \tag{C2}$$

$$E(t) = \sum_{m=0}^{\infty} Z_m [H(t) + B(t)]^{m+1} \tag{C3}$$

$$= \sum_{l=0}^{\infty} \sum_{m=0}^{\infty} Z_m \binom{m+1}{l} [H(t)]^l [B(t)]^{m+1-l}$$

$$= \sum_{k=0}^{\infty} \sum_{l=0}^{\infty} \sum_{m=0}^{\infty} Z_m \binom{m+1}{l} [B(t)]^{m+1-l} [H_0/2]^l \binom{l}{k} e^{\imath(l-2k)\omega_0 t} \rightrightarrows \sum_{k=0}^{\infty} \sum_{m=0}^{\infty} Z_m \binom{m+1}{2k+1} [B(t)]^{m+1-(2k+1)} [H_0/2]^{2k+1} \binom{2k+1}{k} e^{\imath\omega_0 t}$$

$$+ \sum_{k=1}^{\infty} \sum_{m=0}^{\infty} Z_m \binom{m+1}{2k-1} [B(t)]^{m+1-(2k-1)} [H_0/2]^{2k-1} \binom{2k-1}{k} e^{-\imath\omega_0 t}$$

$$= 2\cos(\omega_0 t) \sum_{k=0}^{\infty} \sum_{m=2k}^{\infty} Z_m \binom{m+1}{2k+1} [B(t)]^{m-2k} [H_0/2]^{2k+1} \binom{2k+1}{k}$$

$$= 2\cos(\omega_0 t) \sum_{k=0}^{\infty} \sum_{m=0}^{\infty} Z_{m+2k} \binom{m+2k+1}{2k+1} [H_{ac}(e^{\imath\delta_0 t} + e^{-\imath\delta_0 t})/2]^m [H_0/2]^{2k+1} \binom{2k+1}{k}$$

$$= 2\cos(\omega_0 t) \sum_{m=0}^{\infty} [H_{ac}/2]^m \sum_{l=0}^{\infty} \binom{m}{l} e^{\imath(m-2l)\delta_0 t} \sum_{k=0}^{\infty} Z_{m+2k} \binom{m+2k+1}{2k+1} [H_0/2]^{2k+1} \binom{2k+1}{k}$$

$$= 2\cos(\omega_0 t) \sum_{m=-\infty}^{\infty} e^{\imath m\delta_0 t} \sum_{l=0}^{\infty} [H_{ac}/2]^{m+2l} \binom{m+2l}{l} \sum_{k=0}^{\infty} Z_{m+2l+2k} \binom{m+2l+2k+1}{2k+1} [H_0/2]^{2k+1} \binom{2k+1}{k}$$

$$= 2\cos(\omega_0 t) \sum_{m=-\infty}^{\infty} e^{\imath m\delta_0 t} \bar{E}_m(H_0, H_{ac}), \tag{C4}$$

$$\bar{E}_{2n[+1]}(H_0, H_{ac}) = \sum_{l=\max(n,0)}^{\infty} [H_{ac}/2]^{2l[+1]} \binom{2l[+1]}{l-n} \sum_{k=0}^{\infty} Z_{2l[+1]+2k} \binom{2l[+1]+2k+1}{2k+1} [H_0/2]^{2k+1} \binom{2k+1}{k}$$

$$= \sum_{l=|n|}^{\infty} [H_{ac}/2]^{2l[+1]} \binom{2l[+1]}{l-n} \sum_{k=l}^{\infty} Z_{2k[+1]} \binom{2k[+1]+1}{2(k-l)+1} [H_0/2]^{2(k-l)+1} \binom{2(k-l)+1}{(k-l)}$$

$$= (2|n|[+1]+1) Z_{2|n|[+1]} [H_{ac}/2]^{2|n|[+1]} [H_0/2] + \cdots,$$

$$\binom{2l}{l-m} = \binom{2l}{l+m} \Rightarrow \bar{E}_{2n}(H_0, H_{ac}) = \bar{E}_{2|n|}(H_0, H_{ac}). \tag{C5}$$

*Electronic address: roland.hott@ifp.fzk.de

[1] W. N. Hardy, D. A. Bonn, D. C. Morgan, Ruixing Liang, and Kuan Zhang, Phys. Rev. Lett. **70**, 3999 (1993).

[2] D. C. Mattis and J. Bardeen, Phys. Rev. **111**, 412 (1958).

[3] A. Hosseini, R. Harris, Saeid Kamal, P. Dosanjh, J. Preston, Ruixing Liang, W. N. Hardy, and D. A. Bonn, Phys. Rev. B **60**, 1349 (1999).

[4] H. J. Fink, Phys. Rev. B **58**, 9415 (1998).

[5] P. J. Hirschfeld, W. O. Putikka, and D. J. Scalapino, Phys. Rev. Lett. **71**, 3705 (1993); P. J. Hirschfeld, W. O. Putikka, and D. J. Scalapino, Phys. Rev. B **50**, 10250 (1994).

[6] T. S. Nunner and P. J. Hirschfeld, Phys. Rev. B **72**, 014514 (2005).

[7] Y. Zhang, N. P. Ong, P. W. Anderson, D. A. Bonn, R. Liang, and W. N. Hardy, Phys. Rev. Lett. **86**, 890 (2001).

[8] G. P. Segre, N. Gedik, J. Orenstein, D. A. Bonn, Ruixing Liang, and W. N. Hardy, Phys. Rev. Lett. **88**, 137001 (2002).

[9] B. Batlogg, Solid State Commun. **107**, 639 (1998).

[10] J. Ruvalds, Supercond. Sci. Technol. **9**, 905 (1996).

[11] D. A. Bonn, P. Dosanjh, R. Liang, and W. N. Hardy, Phys. Rev. Lett. **68**, 2390 (1992).

[12] J. R. Waldram, P. Theopistou, A. Porch, and H. M. Cheah, Phys. Rev. B **55**, 3222 (1997).

[13] M. Calandra and O. Gunnarsson, Europhys. Lett. **61**, 88 (2003);

O. Gunnarsson, M. Calandra, and J. E. Han, Rev. Mod. Phys. **75**, 1085 (2003).

[14] T. P. Orlando and K. A. Delin, *Foundations of Applied Superconductivity* (Addison-Wesley Publishing Company, Reading, MA, 1991), p. 111 ff.

[15] H. J. Chaloupka and T. Kässer, in *High Temperature Superconductivity 2-Engineering Applications*, edited by A. V. Narlikar (Springer, Berlin, 2004), p. 411 ff.

[16] M. J. Lancaster, *Passive Microwave Device Applications of High Temperature Superconductors* (Cambridge University Press, Cambridge, 1997), Chaps. 4 and 5.

[17] M. Hein, *High Temperature Superconductor Thin Films at Microwave Frequencies*, Springer Tracts in Modern Physics, Vol. 155 (Berlin, Heidelberg, 1999), Chaps. 3 and 5.

[18] N. Belk, D. E. Oates, D. A. Feld, G. Dresselhaus, and M. S. Dresselhaus, Phys. Rev. B **56**, 11966 (1997).

[19] P. Lahl, R. Wördenweber, and M. A. Hein, Appl. Phys. Lett. **79**, 512 (2001).

[20] T. Dahm and D. J. Scalapino, Phys. Rev. B **60**, 13125 (1999).

[21] B. A. Willemsen, K. E. Kihlstrom, T. Dahm, D. J. Scalapino, B. Gowe, D. A. Bonn, and W. N. Hardy, Phys. Rev. B **58**, 6650 (1998).

[22] J. C. Booth, L. R. Vale, R. H. Ono, and J. H. Claassen, J. Supercond. **14**, 65 (2001).

[23] D. Agassi and D. E. Oates, Phys. Rev. B **72**, 014538 (2005).

[24] A. G. Zaitsev, R. Schneider, G. Linker, F. Ratzel, R. Smithey, and J. Geerk, Appl. Phys. Lett. **79**, 4174 (2001).

[25] A. G. Zaitsev, R. Schneider, G. Linker, F. Ratzel, R. Smithey, and J. Geerk, IEEE Trans. Appl. Supercond. **13**, 336 (2003).

[26] H. Xin, D. E. Oates, G. Dresselhaus, and M. S. Dresselhaus, Phys. Rev. B **65**, 214533 (2002).

[27] D. M. Sheen, S. M. Ali, D. E. Oates, R. S. Withers, and J. A. Kong, IEEE Trans. Microwave Theory Tech. **39**, 1522 (1991).

[28] D. E. Oates, A. C. Anderson, D. M. Sheen, and S. M. Ali, IEEE Trans. Appl. Supercond. **1**, 108 (1991).

[29] J. Halbritter, Supercond. Sci. Technol. **16**, R47 (2003).

[30] Actually, the extraction of $|c_n| \approx [i_{2n+1}(h)]^{1/2}$ at finite h can be justified from numerical estimates of (15), (16), and (20).

[31] N. Belk, D. E. Oates, D. A. Feld, G. Dresselhaus, and M. S. Dresselhaus, Phys. Rev. B **53**, 3459 (1996).

[32] G. D. Poulin, J. S. Preston, and T. Strach, Phys. Rev. B **48**, 1077 (1993).

[33] S. Kolesov, H. Chaloupka, A. Baumfalk, and T. Kaiser, J. Supercond. **10**, 179 (1997).